energies

MDPI

Article

Investigation of Combustion Properties and Soot Deposits of Various US Crude Oils

Gurjap Singh [1,*], Mehdi Esmaeilpour [2] and Albert Ratner [1]

[1] Department of Mechanical Engineering, The University of Iowa, Iowa City, IA 52242, USA; albert-ratner@uiowa.edu
[2] College of Information Technology and Engineering, Marshall University, Huntington, WV 25755, USA; esmaeilpour@marshall.edu
* Correspondence: gurjap-singh@uiowa.edu

Received: 17 May 2019; Accepted: 17 June 2019; Published: 20 June 2019

Abstract: The oil boom in the North Dakota oilfields has resulted in improved energy security for the US. Recent estimates of oil production rates indicate that even completion of the Keystone XL pipeline will only fractionally reduce the need to ship this oil by rail. Current levels of oil shipment have already caused significant strain on rail infrastructure and led to crude oil train derailments, resulting in loss of life and property. Treating crude oil as a multicomponent liquid fuel, this work aims to understand crude oil droplet burning and thereby lead to methods to improve train fire safety. Sub-millimeter sized droplets of Pennsylvania, Texas, Colorado, and Bakken crude were burned, and the process was recorded with charge-couple device (CCD) and complementary metal-oxide semiconductor (CMOS) high-speed cameras. The resulting images were post-processed to obtain various combustion parameters, such as burning rate, ignition delay, total combustion time, and microexplosion behavior. The soot left behind was analyzed using a Scanning Electron Microscope (SEM). This data is expected be used for validation of combustion models for complex multicomponent liquid fuels, and subsequently in the modification of combustion properties of crude oil using various additives to make it safer to transport.

Keywords: crude oil; petroleum; droplet combustion; burning rate; ignition delay; soot deposits; Bakken crude; Pennsylvania crude; Colorado crude; Texas crude

1. Introduction

Recent decades have seen growing energy demand due to the increasing trend of industrialization in the world as well as population growth. Crude oil, or petroleum, is a major source of energy in power generation systems, and most countries import crude oil and its derivatives to cope with their increasing energy demand.

In the United States, new methods of oil exploration (such as fracking) and the exploration of new oil regions (such as Bakken formation in North Dakota) have resulted in crude oil production boom. In 2016, the US became the largest exporter of refined petroleum products [1]. Rail is the primary method of shipping this crude oil (also referred to as just "crude" in this manuscript), since a major pipeline system meant to transport it has been indefinitely delayed [2].

From 2010 to 2015, crude oil shipments from the Midwest to the rest of the US have steadily increased [3]. With rail crude now supplying more than half of the east coast refineries' feedstock [3], the stress on the aging rail infrastructure has been thrown into sharp relief, with many crude oil derailments and crashes in recent years. These generally result in devastating oil fires and loss of life and property [4–6].

Upgrading US rail infrastructure is an expensive and time-intensive undertaking, and, meanwhile, the crude has to be transported to fulfil the nation's energy needs. Therefore, a stop-gap solution must be developed to control the combustion behavior of crude in the event of a derailment. The first step for that is the measurement and quantification of combustion properties of various US crudes, which is one of the objectives of this paper.

The well-established experimental setup used in present research has been previously used to determine combustion characteristics of liquid fuels [7–9] and yields convenient measurement of vital important properties such as ignition delay [9] and burning rates [7–9]. Furthermore, this method is implementable at a lab scale, uses small sample quantities, and promotes spherical symmetry of the droplet as it burns. The latter is important for the eventual mathematical modeling of the combustion process. Treating crude as a multicomponent liquid fuel, this paper establishes the experimental burning rate and ignition delay of sub-millimeter sized droplets of various crudes.

There are several challenges involved with determining the combustion characteristics of crude as a liquid fuel. The physical and chemical properties of crude oils depend on the production lot and the region of origin, which cause variation in crude oil combustion characteristics. Because of its multicomponent nature, the crude oil combustion process runs quite differently compared to a pure single-component liquid fuel. The presence of various hydrocarbons, each with their own viscosity, density, and boiling point, in crude oils present a challenge in the burning mechanism of this fuel [10,11].

The combustion process of this kind of multicomponent fuel can be associated with an unsteady burning process with a sudden fragmentation of fuel droplets, called a microexplosion. A microexplosion in droplet combustion occurs when the droplet's internal temperature exceeds the homogeneous nucleation temperature of a fuel component, which results in the formation and growth of a vapor bubble inside the fuel droplet. The growing vapor bubble ultimately shatters the surrounding liquid fuel into smaller fragments that burn more efficiently. Microexplosions have been widely discussed in literature for multicomponent fuel droplet combustion in normal and reduced gravity [12–19]. Although concerns have been raised on the role of supporting fiber as a nucleation site for bubbling, the microexplosions of fiber-supported droplets have been widely studied [15–19].

Only a few systematic studies of crude oil combustion characteristics appear in the literature, but they are mostly related to pool fires. Iwata et al. [20] studied variations in the burning behavior of crude oils based on small-scale free-burning pool fire data. They conducted tests to measure the heat release rate based on oxygen consumption calorimetry, radiative heat flux from the flame, mass loss rate, liquid fuel temperature, and the concentration of CO_2 and CO in the exhaust gas for various crude oils. They observed that the heat release rate, mass loss rate, and flame radiation were a function of the type of crude oil. The effect of surface area on the in-situ combustion of crude oil was investigated by Drici and Vossoughi [21] through tests on crude oil alone and in the presence of clays, silica, and alumina with variable surface areas. They observed that decreasing the crude oil/surface area ratio enhanced the low-temperature oxidation peak. They also found that additives with a large specific surface area shifted a large portion of the exothermic heat from a higher to a lower temperature range. Kok et al. [22] studied the oxidation of crude oil in a porous medium under pressurized conditions to simulate in-situ combustion during oil recovery using high pressure thermogravimetric analysis (HPTG). They observed three distinct reaction regions from the HPTG curves in an oxidizing environment subjected to a constant heating rate. These were low-temperature oxidation, fuel deposition, and high-temperature oxidation. The method of Coats and Redfern was used to obtain kinetic parameters, and the results were discussed. An investigation of the combustion process of crude oil was performed by Nowak et al. [23]. A top-mounted combustor was scaled down from the baseline system, and different types of crude oil were burnt in the atmospheric test rig. They studied the combustion process by measuring temperature and velocity field distributions in the combustion chamber for different injector designs' parameters. They also measured the molar fraction of CO_2 and compared it to the injector parameters.

The research presented in this work was carried out on crude oil acquired from the Rocky Mountain oil production region (Colorado), the Northern Great Plains oil production region (Bakken-North Dakota), the Northeast oil production region (Pennsylvania), and the Gulf Coast oil production region (Texas). Although there can be significant variety in crude oil properties, Table 1 presents the typical properties of Colorado, Pennsylvania, and Texas crudes from [24] and the typical properties of Bakken crude from [25].

Table 1. Typical properties of crude oils being tested.

Property\Crude Type	Bakken	Colorado	Pennsylvania	Texas
Initial Boiling Point (°C)	21	29	30	73
Specific Gravity	0.815	0.817	0.832	0.855

The main goal of the research presented in the work is to gain knowledge of the crude oil combustion mechanism. An analysis of the results of the burning rate, ignition time, and microexplosion behavior at the scale of a single spherical fuel droplet is presented in this work. This research has been formulated to lay the groundwork for the eventual modification of crude combustion behavior using physical and chemical means to improve transportation safety. Various nanomaterials [8,9] and polymeric additives [7] are envisioned to be used in the future to bring about such combustion behavior modifications.

2. Experimental Procedure

The experimental apparatus was inspired by the original work of Avedisian et al. [26] and Bae et al. [27] and was previously used in the work presented by Singh et al. [9]. Three 16 µm silicon-carbide (SiC) fibers are fixed between six posts, as shown in Figure 1. A sub-millimeter-sized droplet is suspended at the center point of the fibers. The upper limit to the initial size of the droplets (or d_0) is kept sub-millimeter because larger droplets cannot be supported by the support fibers. Droplet size was also influenced by the need to exceed the criteria described by Avedisian and Jackson [28] to keep (d_0/d_{fiber}) >13 to match burning rates close to those of unsupported droplets. For the present study, a ratio of 60 > (d_0/d_{fiber}) > 48 was maintained.

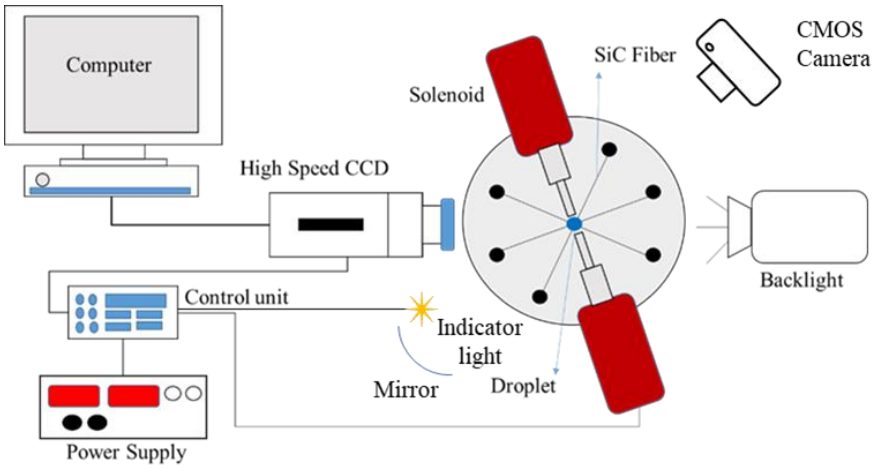

Figure 1. Schematic of experimental setup for crude oil combustion.

Semi-circular heating coils of 1 mm diameter are positioned in close proximity on either side of the droplet. These coils are made of 36 gauge Kenthal with a resistance of 4 Ω each and are connected to a power supply of 15 V to make them glow red-hot. Combined, they produce energy equivalent to 14.06 J in a typical experiment where they are energized for 500 ms. The coils are mounted on the end-effectors of solenoids. A microcontroller (Arduino Uno), in sync with the high-speed camera,

waits for a signal from the computer when the process is to be initiated. Upon receiving the signal, it further signals the coils to glow for a pre-determined time (typically 500 ms as previously noted) and start the combustion process. The process of droplet combustion is captured by a black and white IDT X-StreamVision XS-3 CCD camera operated at 1000 frames per second and fitted with a 105 mm lens (Nikon AF Micro-Nikkor-F/2.8, Tokyo, Japan). Back-lighting is provided by a single bright white LED at 3.3 V.

Simultaneously, the combustion event is magnified with a concave mirror (4.0″ diameter, 9.0″ focal length) and recorded with a Casio EXILIM Pro EX-F1 CMOS camera (Casio, Tokyo, Japan) at 600 frames per second. As the coils are signaled to start glowing, an indicator light (bright white LED) is switched on by the microcontroller at the same time. The field of view of the CMOS camera is large enough to capture both the combustion process and the indicator light. The obtained color video footage is post-processed using MATLAB®(MathWorks, Natick, MA, USA) to extract all frames sequentially. The images obtained are 8-bit/channel RGB frames with 432 × 192 pixels resolution. There is a delay of 1.7 ms between two consecutive frames, so the exact time between the indicator light switching on and the combustion process starting can be calculated by counting the number of frames between the two processes. Similarly, total combustion time can also be calculated.

The CCD camera yields 8-bit grayscale images with 948 × 592 pixels resolution. To obtain the size of the droplet, the combustion process CCD camera images are post-processed using Fiji/ImageJ, an open-source digital image processing software developed by several laboratories [29–31]. The SiC suspending wires are so small that a typical droplet starts out almost perfectly spherical. As combustion progresses, there are microexplosions within the droplet that distort its shape, so a corrective procedure is done to calculate equivalent diameter [8,32,33]:

$$d_{eff} = \sqrt[3]{d_{max} d_{min}^2} \quad (1)$$

where d_{max} and d_{min} are the major and minor droplet diameters. As stated earlier, crude oil samples from various US oil fields (identified as Colorado, Bakken-North Dakota, Pennsylvania, and Texas) were obtained for this research. All samples obtained were light and sweet paraffinic types.

3. Results and Discussion

In all the samples tested during this study, most of the combustion process is marked by the presence of microexplosions (Figure 2). The beginning of the experimental process consists of the ignition coils heating the droplet, which leads to volumetric expansion. This is marked by an increase in normalized droplet area $(d/d_0)^2$ in Zone I (Figures 3–5) and has been reported in the literature before by Singh et al. [9]. Since the droplet is being heated but does not catch fire until the end of Zone I, this zone is also termed ignition delay. The end of Zone I is marked by a decrease in normalized droplet area $(d/d_0)^2$.

After ignition has been achieved, the general behavior of all crude oils is steady combustion with the added component of puffing and microexplosions for most of the duration of their combustion. However, several distinct zones were evident and will be explained in the subsequent sections. Bakken, Colorado, and Pennsylvania crude oils show almost the same behavior. As explained above, there is a swell in the droplet as it expands due to heating. As combustion is initiated and the fuel vaporizes to burn in the flame, the droplet shrinks. At the start of the combustion process, there is a period of steady burning accompanied by a few microexplosions (Zone II), which gives way to a period of violent microexplosions (Figure 2) in Zone III, which then gives way to a period of steadier burning with smaller-intensity microexplosions in Zone IV (Figures 3–5). All these combustion regimes can be classified as distinct zones.

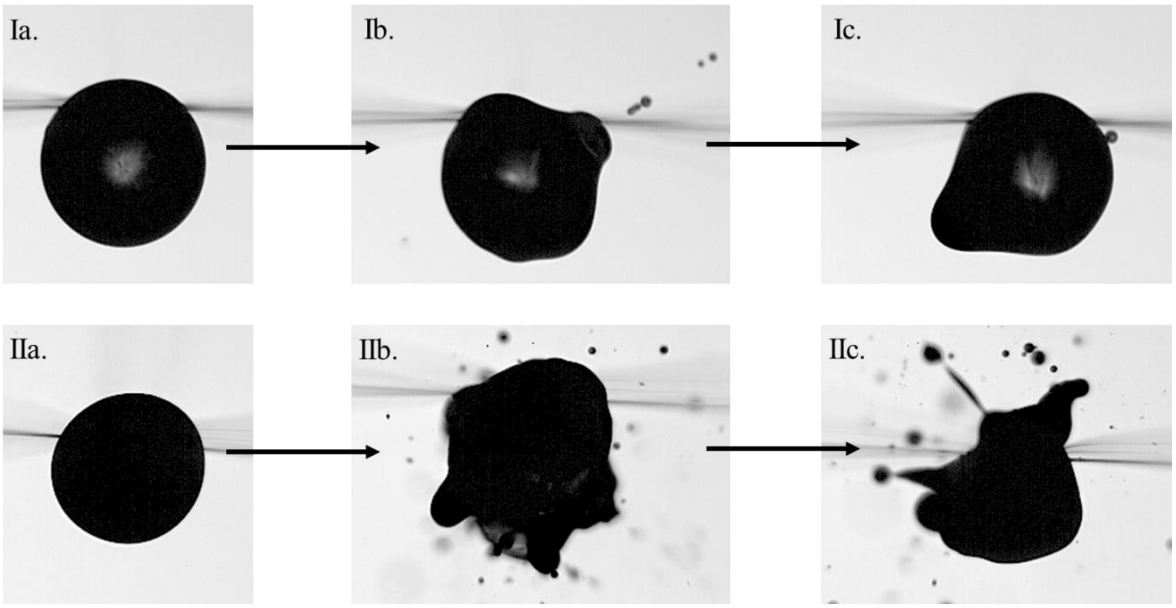

Figure 2. High-speed camera images showing distortion and microexplosions in Colorado (Ia, Ib, Ic) and Texas (IIa, IIb, IIc) crudes.

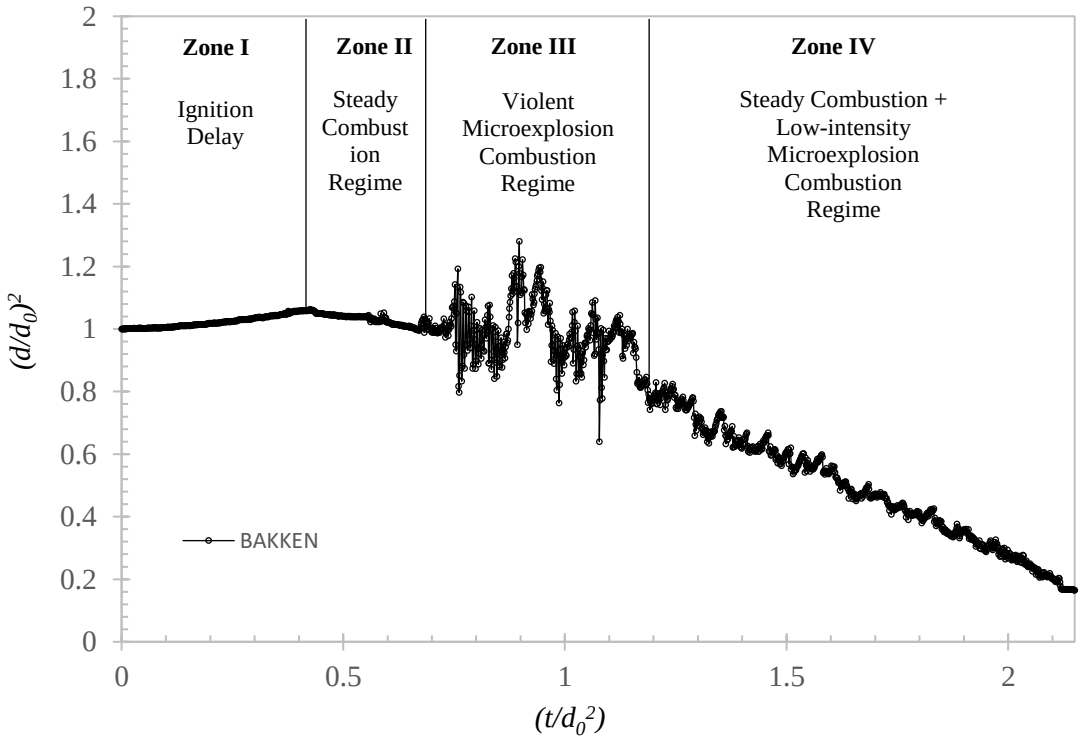

Figure 3. The evolution of $(d/d_0)^2$ with time for Bakken crude oil with various combustion zones ($d_0 = 0.783mm$).

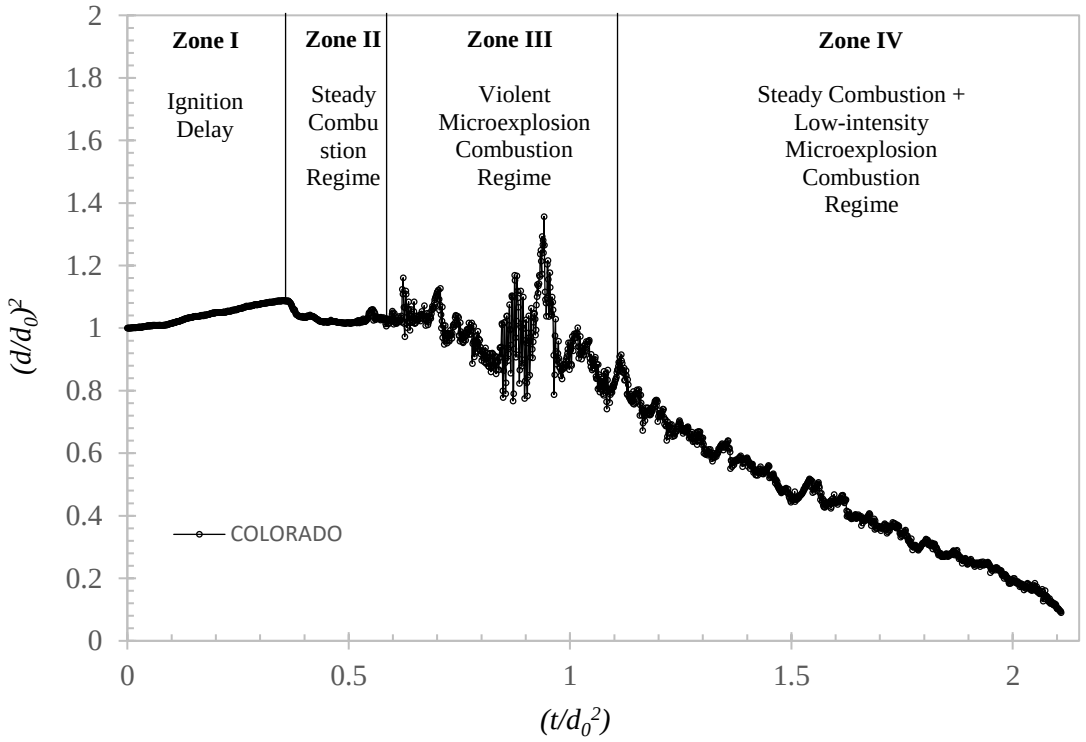

Figure 4. The evolution of $(d/d_0)^2$ with time for Colorado crude oil with various combustion zones ($d_0 = 0.855mm$).

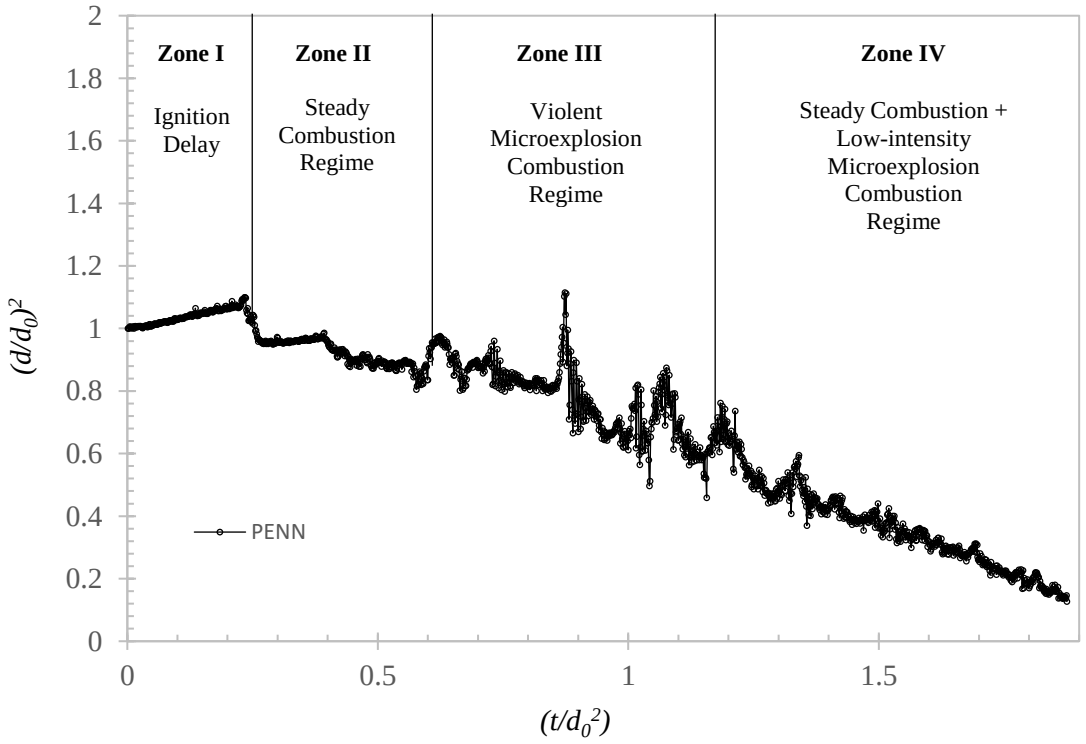

Figure 5. The evolution of $(d/d_0)^2$ with time for Pennsylvania crude oil with various combustion zones ($d_0 = 0.79mm$).

This combustion behavior can be explained by the highly multicomponent nature of crude oil. Crude oil consists of different components that boil at low, intermediate, and high temperatures. In the beginning, the droplet is relatively cold, and Zone II burns steadily with very few microexplosions

because there is very little differential boiling. As combustion progresses, the low and intermediate fractions start to bubble and evaporate, causing a large amount of microexplosions, as seen in Zone III. As these components bubble out and escape, and the droplet temperature continues going up, only fractions that have higher boiling points are left, for the most part, and a steadier combustion regime with lower microexplosion intensity is seen in Zone IV.

Texas crude oil burns aggressively from beginning to the end, with violent microexplosions. This can be attributed to the presence of water with a boiling point, as well as presence of the other low-boiling components in this crude. The burning properties of Texas crude pose substantial problems for accurate image processing to obtain reliable burning rates. Therefore, burning rates have only been calculated for Bakken, Pennsylvania, and Colorado crudes.

Unless otherwise noted, at least five experiments were performed for each crude. After post processing, the average of the combustion rates, microexplosion behavior, ignition delay, and total combustion time from these experiments yielded the general combustion properties of that particular fuel, with the standard deviation serving as the error.

3.1. Burning Rate of Fuel Droplets

Bakken, Colorado, and Pennsylvania crudes show several distinct combustion zones (Figures 3–5). Zone IV (Steady Combustion + Low-intensity Microexplosion Combustion Regime) shows a much clearer and meaningful combustion trend than Zone III (Violent Microexplosion Combustion Regime). Zone IV also comprises a significant amount, if not the majority, of the total combustion regime in all experiments conducted with Bakken, Colorado, and Pennsylvania crudes. For this reason, only the Zone IV burning rates have been calculated for these crudes. Zone IV is non-existent for Texas crude because the entirety of that crude oil type is spent in Zone III; this is discussed further in the following section, which outlines the microexplosion characteristics of all fuel types. As droplet combustion progresses, the heat from the flame causes more fuel to evaporate from the droplet surface. This vaporized fuel then burns in the flame. The overall effect is a shrinkage in the droplet diameter, which, in this research, was recorded using a high-speed camera at 1000 frames per second. The variation of diameter d at a given time t follows the well-known quasi-steady theory of droplet combustion, which can be calculated as [34,35]:

$$\frac{d(t)^2}{d_0^2} = 1 - K(\frac{t}{d_0^2}) \quad (2)$$

where $d(t)$ is the diameter of droplet at time t, d_0 is the initial droplet diameter, and K is the combustion or burning rate. It can be seen from Equation (2) that the higher the K, the faster the droplet burns. The moving averaging method was used to reduce data from the original dataset, and the reduced data was used to calculate the combustion rate. At least five experiments were conducted for each fuel type, and the combustion rate for each experiment was calculated separately. An average of all experiments conducted for a single fuel yielded the average combustion rate for that fuel, and the standard deviation for the same served as the error for the calculation (Figure 6). It was found that the combustion rates of Bakken, Colorado, and Pennsylvania crudes are very close (Figure 6). Nominally, Pennsylvania crude was found to be the fastest burning of the three, and Bakken crude was found to be the slowest.

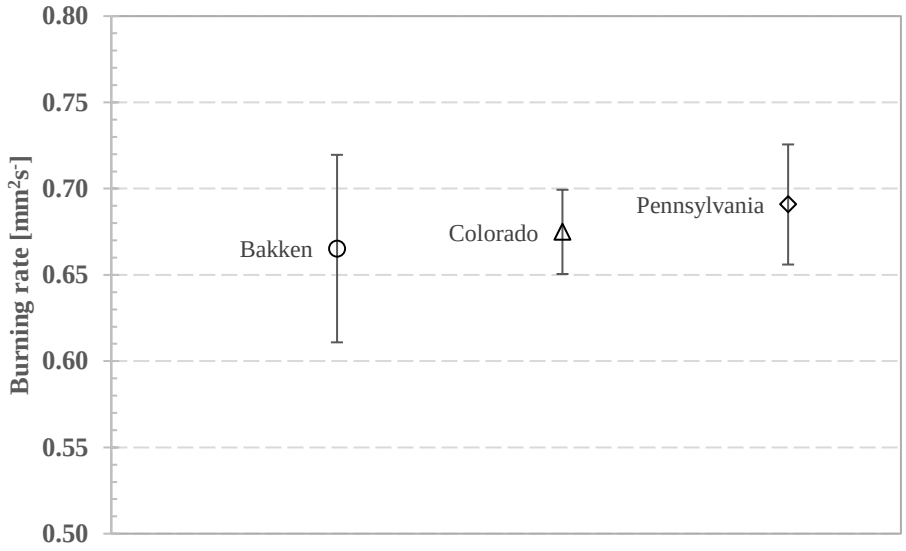

Figure 6. Combustion rates of Bakken, Colorado, and Pennsylvania crude oils in a steady combustion zone.

3.2. Microexplosion Behavior

Microexplosions during droplet combustion are characterized by two phases: puffing and explosion (Figure 7). During puffing, small bubbles form and build up inside the droplet. As stated before, these bubbles comprise the low-boiling-point fractions in the crude oil. For the most part, nucleation is homogeneous throughout the volume of the fluid (Figure 8), as found by Lasheras et al. [36]. The interaction between the bubbles is difficult to quantify because the process is very fast and visibility is limited, but they appear to travel one by one to the droplet surface. Once they arrive at the droplet surface, they pop, releasing hot and readily combustible vapor to the flame. This results in an explosion that causes the whole droplet to distort and smaller droplets to be ejected; this event is termed a "microexplosion." Droplet distortion due to microexplosions can sometimes entrain bubbles into the liquid bulk, consistent with previous research by Wang et al. [37], which suggests that air entrainment can contribute to microexplosions. The puffing and explosion phenomena can be observed as a rapid spike and dip, respectively, in the evolution of the $(d/d_0)^2$ data of a given droplet (Figures 3–5). Avedisian et al. [34] described two sorts of microexplosions: "balloon burst" and "spitting." Bakken, Pennsylvania, and Colorado crudes display the spitting microexplosion, while Texas crude displays both spitting and balloon burst microexplosions (Figure 9). In comparison to these multicomponent fuels, note that single-component fuels, such as soy-based biodiesel, displayed very little to no microexplosions [9].

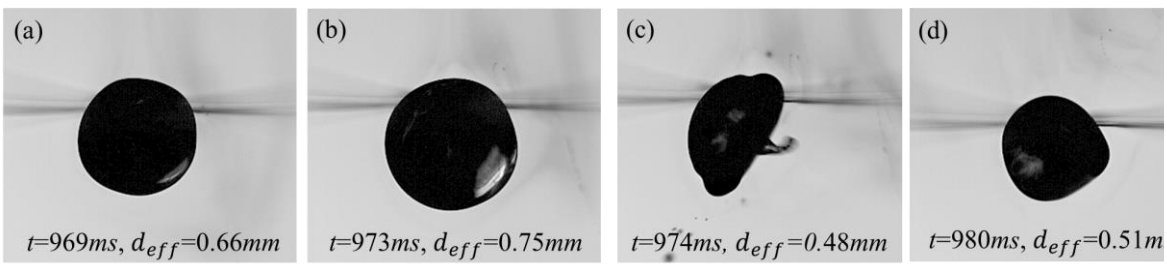

Figure 7. Microexplosion progression in a Bakken crude oil droplet, along with effective diameter, d_{eff} (see Equation (1)). Puffing from (**a**) to (**b**), a microexplosion in (**c**), and the shrunken droplet with a smaller effective diameter in (**d**).

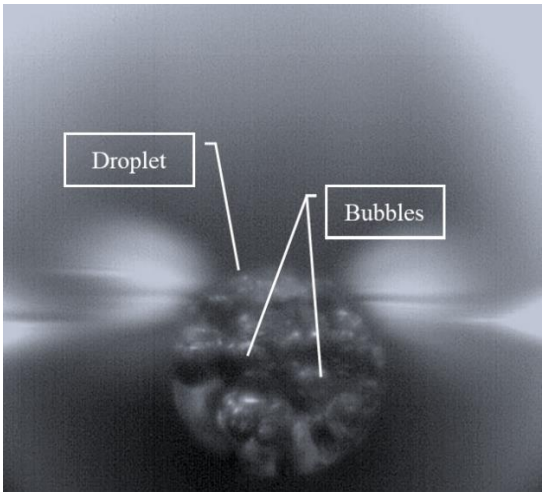

Figure 8. The imaging of a Colorado crude oil droplet with homogeneous bubble nucleation and growth inside the fuel droplet.

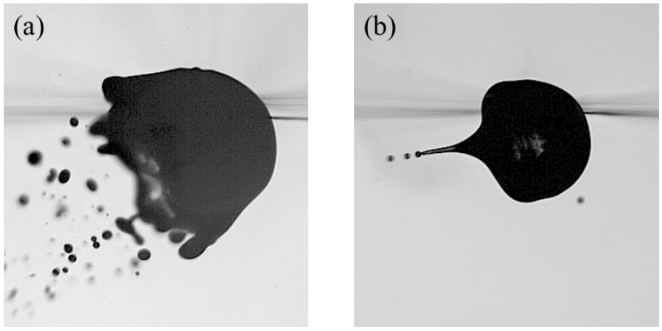

Figure 9. High-speed imaging of (**a**) Texas crude oil showing a balloon burst microexplosion and (**b**) Bakken crude oil showing a spitting microexplosion.

The puffing and explosion phenomena can be observed as a rapid spike and dip, respectively, in the evolution of $(d/d_0)^2$ data of a given droplet (see Figure 10). This information can be used to characterize microexplosion intensity. A single microexplosion, as shown in Figure 10, is characterized by a local maxima with a local minima in the $(d/d_0)^2$ plot. The puffing process takes place from (a) to (b) and is characterized by a sharp rise in $(d/d_0)^2$. The explosion takes place from (b) to (c) and is marked by a sharp decrease in $(d/d_0)^2$. A stronger, more intense, microexplosion can, therefore, be characterized by having a sharper puffing and/or a sharper explosion region in a given amount of time. Microexplosion intensity for a given microexplosion event can, therefore, be quantified as:

$$I = [(y_b - y_a) + (y_b - y_c)]/(x_c - x_a) \quad [1/s] \tag{3}$$

where I is the intensity of the microexplosion event, $y = (d/d_0)^2$, and $x = t$.

The intensity of microexplosion events for Zone III for all experiments was calculated. The average number of microexplosion events and intensity for each fuel was then calculated, as well as the standard deviation. The latter served as the error for these calculations (Figure 11). Texas crude surpassed all other crudes in average intensity of microexplosions, which also attests to the highly explosive burning behavior captured by the CCD and CMOS cameras. Among the Bakken, Pennsylvania, and Colorado crudes, Bakken has the highest average microexplosion intensity.

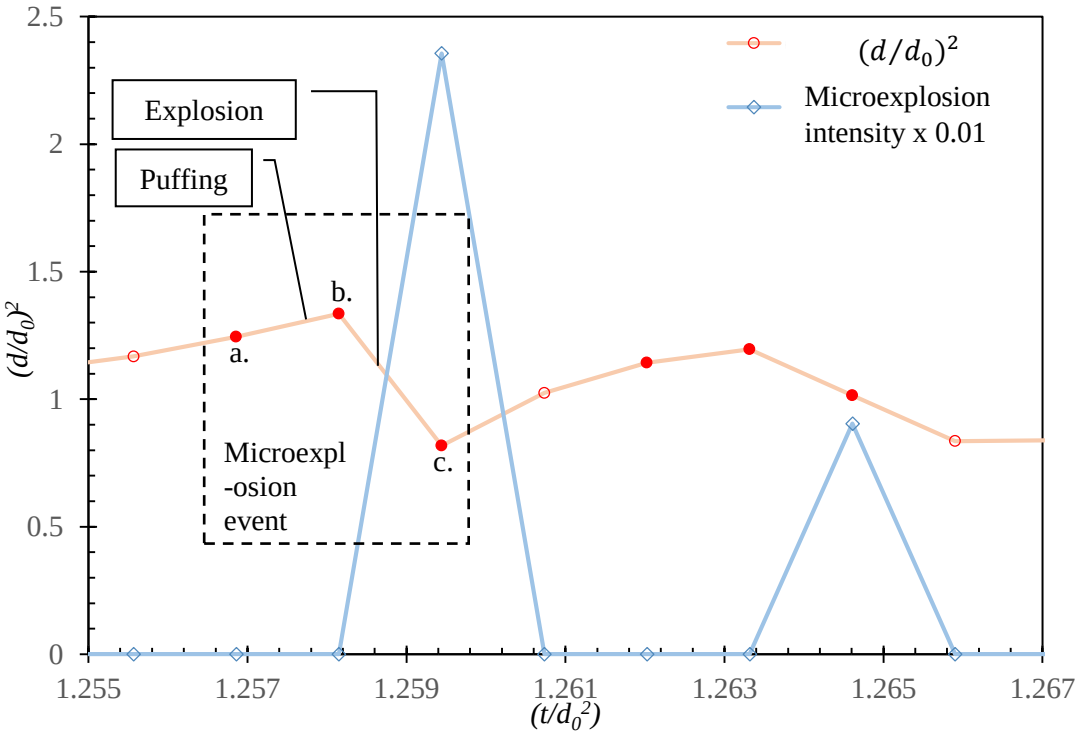

Figure 10. Microexplosion behavior in a Bakken crude droplet experiment, zoomed into the region from $t/d_0^2 = 1.25$ to 1.267 to show microexplosion characterization and intensity (scaled by a factor of 100 for easier representation). Solid red points correspond to the $(d/d_0)^2$ plot points that characterize puffing and explosion behavior. A single microexplosion event progresses from a to b to c. Region a to b represents droplet puffing, marked by a sharp rise in normalized droplet area $(d/d_0)^2$, which is followed by an explosion from b to c, characterized by a sharp decrease in $(d/d_0)^2$.

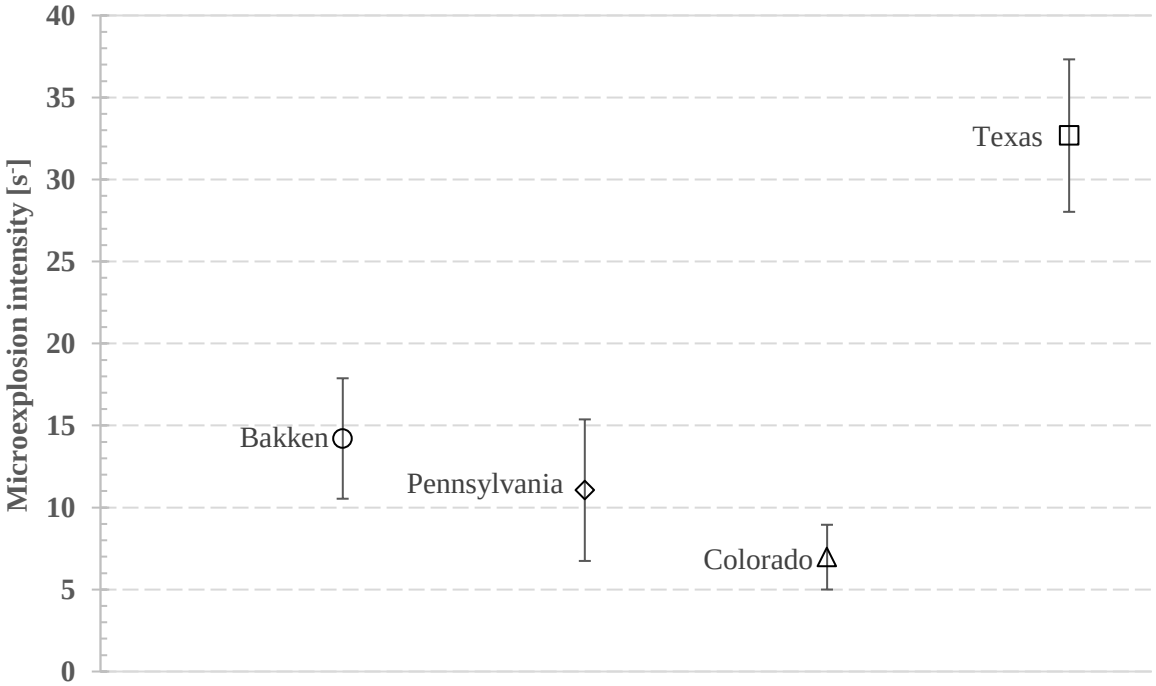

Figure 11. The average microexplosion intensity for various crude oils in Zone III.

3.3. Ignition Delay Time

Ignition delay is the time a given fuel droplet takes to start burning after heating coils have been activated. It measures how easily a given fuel droplet will ignite—the smaller the ignition delay, the easier it is to ignite the fuel. Ignition delay time was measured using footage obtained from the CMOS camera, with data input from the CCD camera. A MATLAB code was used to extract all frames from the CMOS footage, and the number of frames between the heating coils being activated and the combustion process starting was counted. Since the footage was recorded at 600 frames per second, the time difference between any two consecutive frames is about 1.7 ms. Texas crude oil was found to have the maximum average ignition delay of all crudes tested (Figure 12). This can be explained by its higher initial boiling point and higher specific gravity (Table 1) compared to the other crudes. Together with its high microexplosion intensity (Section 3.2), this also points towards the presence of a relatively high water-content in Texas crude, which is common in many crude oils. Bakken crude had the smallest average ignition delay in all crudes tested (Figure 12). This can be explained by the very light nature of this crude oil, with a low initial boiling point and low specific gravity (Table 1), which points to the presence of a large number of low-boiling constituents. Operator error caused ignition delay experimental data to be available for only three experiments for Bakken, leading to a smaller error bar for that crude. Note that these data cannot be supplemented with additional data at this time, since ignition delay is highly sensitive to heating coil size and shape, and the heating coil for this experimental set is not available anymore.

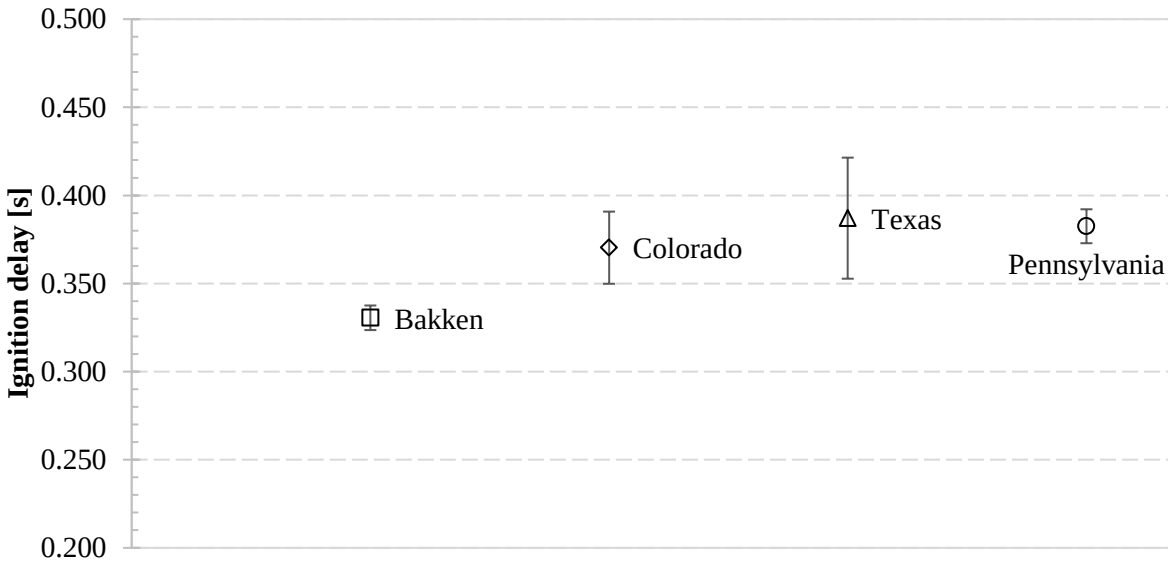

Figure 12. Average ignition delay for different crude oils.

3.4. Total Combustion Time

The technique to measure total combustion time is the same as that used to measure ignition delay. However, frames are counted between combustion initiation and combustion extinction. According to Figure 13, Colorado crude oil burns the longest. Due to its highly explosive and aggressive nature, Texas crude is found to nominally have the smallest total combustion time. This is misleading because most of the volume of the fuel escapes via microexplosions, and neither camera has a field of view large enough to account for all of it. Therefore, in a meaningful way, Bakken crude has the least total combustion time. This is due to its relatively high microexplosion intensity, leading to relatively high liquid loss. Notably, total combustion time experimental data for only two experiments was available for Bakken, leading to a smaller error bar for that crude.

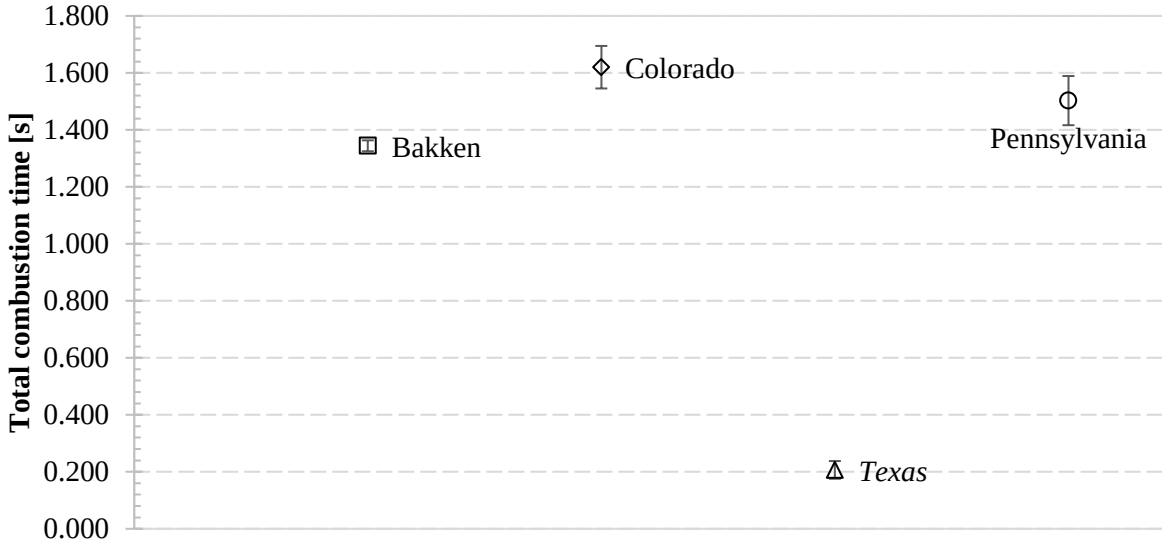

Figure 13. Average total combustion time of different crude oils.

3.5. Soot Residue Analysis

Figure 14 shows the flame structure of a Pennsylvania crude oil droplet, where soot incandescence is visible in the upper regions of the flame. It is also found that Bakken, Colorado, and Pennsylvania crudes leave a soot residue on the supporting fiber after the combustion process has stopped. This soot residue which can be further analyzed to gain more information about the combustion process. Another advantage of soot residue analysis is to find the particulate size in the emissions that can be expected to result from a crude oil fire. This can help determine the appropriate respiratory equipment for fire damage control crews. As shown in Figure 9, Texas crude fluid volume mostly escapes via microexplosions and leaves no soot residue behind. All soot residue samples were tested using a Hitachi S-4800 SEM at the Central Microscopy Research Facility at the University of Iowa.

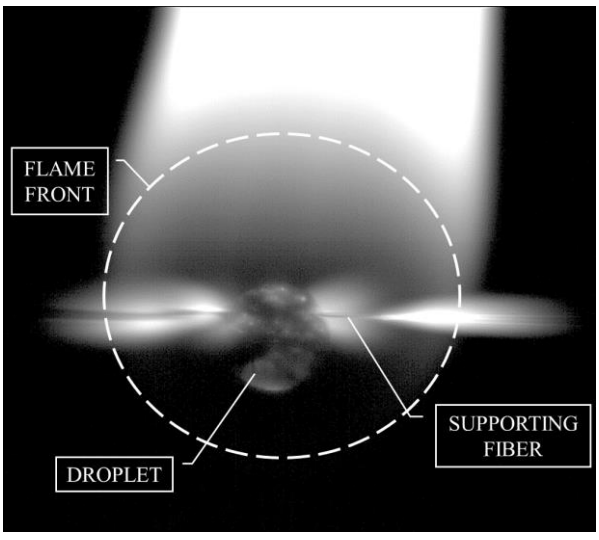

Figure 14. Flame structure of a Pennsylvania crude oil droplet.

Figure 15 shows a representative soot sample from a Colorado crude oil combustion experiment. The SiC support wire can be clearly seen, along with the soot deposited on it. The SEM can zoom into the surface of the soot deposit, where individual soot particles are visible. However, the instrument is limited by the electric conductivity of the sample, and finely resolving very small structures (such as in Figure 16IIb) can be challenging. Figure 16 compares the soot structures of Bakken, Pennsylvania, and

Colorado crude oils. Bakken and Colorado crudes leave behind a spongy, high porosity soot structure with almost spherical individual soot particles with an average size of ~70 µm. Pennsylvania crude leaves behind a more compact spongy soot structure where string-like elements are clearly visible (Figure 16IIa). The individual soot particles average ~20 µm. Ultimately, the soot residue and its structure are highly dependent on the chemical makeup of the fuel.

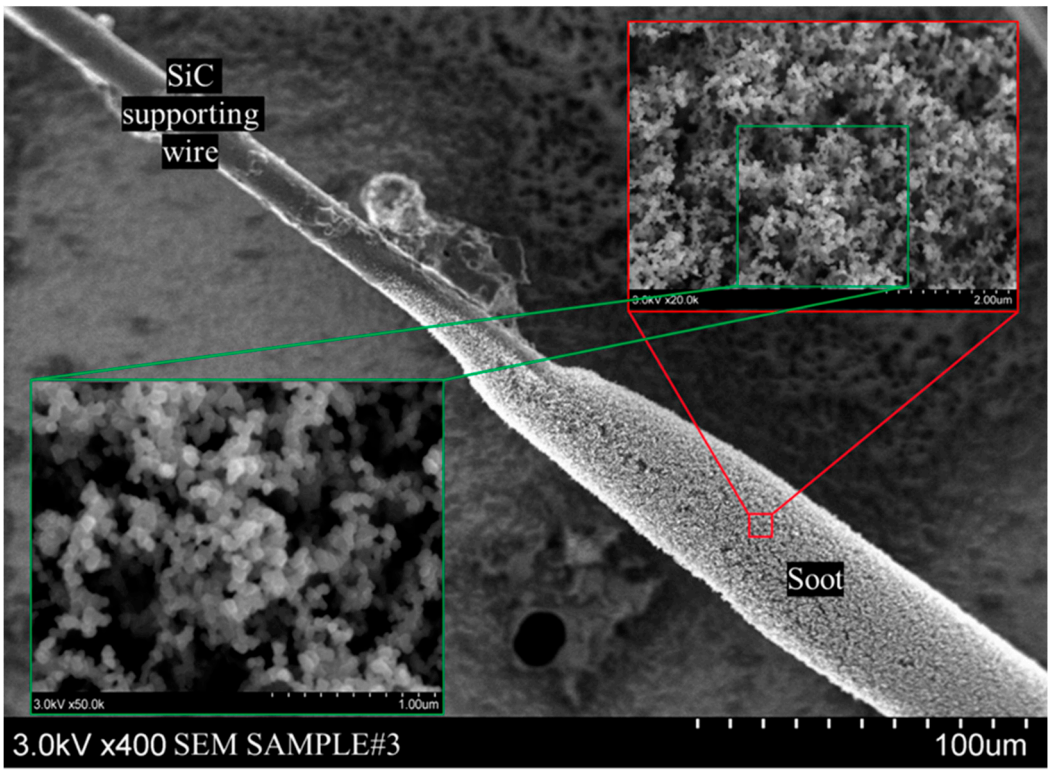

Figure 15. Soot sample from Colorado crude oil combustion experiment shown at various stages of magnification.

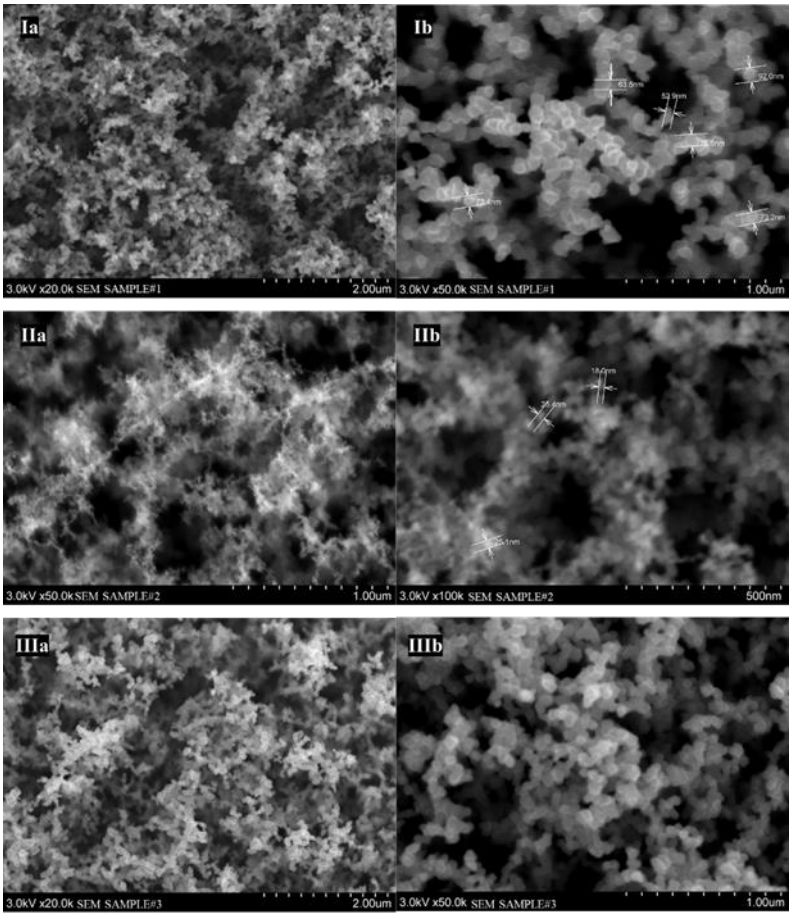

Figure 16. Soot samples at various magnifications; (I) Bakken crude oil, (II) Pennsylvania crude oil, and (III) Colorado crude oil.

4. Conclusions

The study focused mainly on fuel droplet combustion and ignition analysis to compare the burning behavior of four different crude oils at atmospheric pressures and temperatures. Various properties, such as combustion rate, microexplosion intensity, ignition delay, total combustion time, and sooting behavior were presented and discussed.

- Bakken, Pennsylvania, and Colorado crude oils burned with four different combustion regimes, whereas Texas crude oil burned very explosively.
- For the largest and most dominant combustion regime, burning rates for all crudes were found to be comparable. Nominally, Pennsylvania crude burned the fastest and Bakken crude burned the slowest.
- Texas crude was found have the most intense microexplosions of all crudes tested.
- Texas crude also had the highest ignition delay, while Bakken had the lowest. Colorado crude had the highest total combustion time, and Bakken had the lowest.
- Soot analysis with SEM revealed that Bakken and Colorado crudes left a loose, spongy soot residue with individual soot particle sizes of 70 μm, but Pennsylvania crude left behind a more densely packed structure with much smaller average soot particle sizes of 20 μm. This can be attributed to the difference in the chemical compositions of these mixtures.

Properties, such as burning rate, are envisioned to be used in future work to validate numerical combustion models of complex multicomponent liquid fuels. It is expected that this research will

also generate interest in exploring the combustion behaviors of other crude oil types and how best to modify them.

Author Contributions: Conceptualization, G.S.; Data curation, M.E.; Funding acquisition, A.R.; Investigation, G.S.; Methodology, G.S. and M.E.; Project administration, A.R.; Software, M.E.; Supervision, A.R.; Writing—original draft, G.S. and M.E.

Funding: This research is funded, in part, by the Mid-America Transportation Center via a grant from the U.S. Department of Transportation's University Transportation Centers Program, and this support is gratefully acknowledged. The USDOT UTC grant number for MATC is: 69A3551747107.

Acknowledgments: The authors would like to acknowledge use of the University of Iowa Central Microscopy Research Facility, a core resource supported by the Vice President for Research & Economic Development; the Holden Comprehensive Cancer Center; and the Carver College of Medicine. We would especially like to thank Jianqiang Shao for his help and support. The contents reflect the views of the authors, who are responsible for the facts and the accuracy of the information presented herein and are not necessarily representative of the sponsoring agencies, corporations, or persons.

Conflicts of Interest: The authors declare no conflict of interest.

References

1. Central Intelligence Agency. Country Comparison: Refined Petroleum Products-Exports. Available online: https://www.cia.gov/library/publications/resources/the-world-factbook/rankorder/2247rank.html (accessed on 19 June 2019).
2. United States Department of State Final Supplemental Environmental Impact Statement for the KEYSTONE XL PROJECT. January 2014. Available online: https://2012-keystonepipeline-xl.state.gov/documents/organization/221135.pdf (accessed on 19 June 2019).
3. US Energy Information Administration. *Crude by Rail Accounts for More than Half of East Coast Refinery Supply in February*; US Energy Information Administration: Washington, DC, USA, 2015.
4. Nunez, C. *Oil Train Derails in Lynchburg, Virginia*; National Geographic: Washington, DC, USA, 2014.
5. Seville, L.R. *Heimdal, North Dakota, Evacuated After Fiery Oil Train Crash*; NBC News: New York, NY, USA, 2015.
6. Hernandez, T. *Oil Train Derails near Mosier in Oregon's Columbia River Gorge*; The Oregonian: Portland, OR, USA, 2016.
7. Ghamari, M.; Ratner, A. Combustion characteristics of diesel and Jet-A droplets blended with polymeric additive. *Fuel* **2016**, *178*, 63–70. [CrossRef]
8. Ghamari, M.; Ratner, A. Combustion characteristics of colloidal droplets of jet fuel and carbon based nanoparticles. *Fuel* **2017**, *188*, 182–189. [CrossRef]
9. Singh, G.; Esmaeilpour, M.; Ratner, A. The effect of acetylene black on droplet combustion and flame regime of petrodiesel and soy biodiesel. *Fuel* **2019**, *246*, 108–116. [CrossRef]
10. Fingas, M.F. Oil and Petroleum Evaporation. In Proceedings of the 34th Arctic and Marine Oilspill Program Technical Seminar, Vancouver, BC, Canada, 4–6 October 2011; pp. 426–459.
11. Fingas, M.F. *Introduction to Oil Chemistry and Properties, Oil Spill Science and Technology*; Gulf Professional Publishing: Oxford, UK, 2011; pp. 51–59.
12. Wang, C.H.; Liu, X.Q.; Law, C.K. Combustion and microexplosion of freely falling multicomponent droplets. *Combust. Flame* **1984**, *56*, 175–197. [CrossRef]
13. Yap, L.T.; Kennedy, I.M.; Dryer, F.L. Disruptive and micro-explosive combustion of free droplets in highly convective environments. *Combust. Sci. Technol.* **1984**, *41*, 291–313. [CrossRef]
14. Yang, J.C.; Jackson, G.S.; Avedisian, C.T. Combustion of unsupported methanol/dodecanol mixture droplets at low gravity. *Symp. Int. Combust.* **1991**, *23*, 1619–1625.
15. Pan, K.L.; Li, J.W.; Chen, C.P.; Wang, C.H. On droplet combustion of biodiesel fuel mixed with diesel/alkanes in microgravity condition. *Combust. Flame* **2009**, *156*, 1926–1936. [CrossRef]
16. Pan, K.L.; Chiu, M.C. Droplet combustion of blended fuels with alcohol and biodiesel/diesel in microgravity condition. *Fuel* **2013**, *113*, 757–765. [CrossRef]
17. Hou, S.S.; Rizal, F.M.; Lin, T.H.; Yang, T.Y.; Wan, H.P. Microexplosion and ignition of droplets of fuel oil/bio-oil (derived from lauan wood) blends. *Fuel* **2013**, *113*, 31–42. [CrossRef]

18. Rao, D.C.K.; Syam, S.; Karmakar, S.; Joarder, R. Experimental investigations on nucleation, bubble growth, and micro-explosion characteristics during the combustion of ethanol/Jet A-1 fuel droplets. *Exp. Therm. Fluid Sci.* **2017**, *89*, 284–294. [CrossRef]
19. Meng, K.; Wu, Y.; Lin, Q.; Shan, F.; Fu, W.; Zhou, K.; Liu, T.; Song, L.; Li, F. Microexplosion and ignition of biodiesel/ethanol blends droplets in oxygenated hot co-flow. *J. Energy Inst.* **2018**. [CrossRef]
20. Iwata, Y.; Koseki, H.; Janssents, M.I.; Takahashi, T. Combustion Characteristics of Crude Oils. *Fire Mater.* **2001**, *25*, 1–7. [CrossRef]
21. Drici, O.; Vossoughi, S. Study of the Surface Area Effect on Crude Oil Combustion by Thermal Analysis Techniques. *J. Pet. Technol.* **1985**, *37*, 731–735. [CrossRef]
22. Kök, M.; Hughes, R.; Price, D. Combustion characteristics of crude oil-limestone mixtures: High pressure thermogravimetric analysis and their relevance to in-situ combustion. *J. Therm. Anal.* **1997**, *49*, 609–615. [CrossRef]
23. Nowak, D.; Dobski, T.; Slefarski, R.; Jankowski, R.; Magni, F. Experimental studies of crude oil combustion in a top-mounted silo combustor. In Proceedings of the ASME Turbo Expo 2011: Turbine Technical Conference and Exposition, American Society of Mechanical Engineers, Vancouver, BC, Canada, 6–10 June 2011.
24. Smith, N.A.C.; Lane, E.C. *Tabulated Analyses of Representative Crude Petroleums of the United States*; Bureau of Mines, Department of Commerce, United States Government: Washington, DC, USA, 1928.
25. Auers, J.R.; Couture, R.M.; Sutton, D.L. The North Dakota Petroleum Council Study on Bakken Crude Properties. *Accessed Febr.* **2014**, *25*, 2016.
26. Avedisian, C.T.; Callahan, B.J. Experimental study of nonane/hexanol mixture droplet combustion without natural or forced convection. *Proc. Combust. Inst.* **2000**, *28*, 991–997. [CrossRef]
27. Bae, J.; Avedisian, C. Experimental study of the combustion dynamics of jet fuel droplets with additives in the absence of convection. *Combust. Flame* **2004**, *137*, 148–162. [CrossRef]
28. Avedisian, C.T.; Jackson, G.S. Soot patterns around suspended n-heptane droplet flames in a convection-free environment. *J. Propuls. Power* **2000**, *16*, 974–979. [CrossRef]
29. Schindelin, J.; Arganda-Carreras, I.; Frise, E.; Kaynig, V.; Longair, M.; Pietzsch, T.; Preibisch, S.; Rueden, C.; Saalfeld, S.; Schmid, B.; et al. An open-source platform for biological-image analysis. *Nat. Methods* **2012**, *9*, 676–682. [CrossRef]
30. Schneider, C.A.; Rasband, W.S.; Eliceiri, K.W. NIH Image to ImageJ: 25 years of image analysis. *Nat. Methods* **2012**, *9*, 671–675. [CrossRef]
31. Schindelin, J.; Rueden, C.T.; Hiner, M.C.; Eliceiri, K.W. The ImageJ ecosystem: An open platform for biomedical image analysis. *Mol. Reprod. Dev.* **2015**, *82*, 518–529. [CrossRef]
32. Hicks, M.C.; Nayagam, V.; Williams, F.A. Methanol droplet extinction in carbon dioxide-enriched environments in microgravity. *Combust. Flame* **2010**, *157*, 1439–1445. [CrossRef]
33. Struk, P.; Ackerman, M.; Nayagam, V.; Dietrich, D. On calculating burning rates during fiber supported droplet combustion. *Microgravity Sci. Technol.* **1998**, *11*, 144–151.
34. Jackson, G.S.; Avedisian, C.T. Combustion of unsupported water-in-n- heptane emulsion droplets in a convection-free environment. *Int. J. Heat Mass Transf.* **1998**, *41*, 2503–2515. [CrossRef]
35. Glassman, I.; Yetter, R.A.; Glumac, N.G. *Combustion*; Academic press: Cambridge, MA, USA, 2014.
36. Lasheras, J.C.; Fernandez-Pello, A.C.; Dryer, F.L. Experimental observations on the disruptive combustion of free droplets of multicomponent fuels. *Combust. Sci. Technol.* **1980**, *22*, 195–209. [CrossRef]
37. Wang, C.H.; Hung, W.G.; Fu, S.Y.; Huang, W.C.; Law, C.K. On the burning and microexplosion of collision-generated two-component droplets: Miscible fuels. *Combust. Flame* **2003**, *134*, 289–300. [CrossRef]

© 2019 by the authors. Licensee MDPI, Basel, Switzerland. This article is an open access article distributed under the terms and conditions of the Creative Commons Attribution (CC BY) license (http://creativecommons.org/licenses/by/4.0/).